



# HHS Public Access

Author manuscript

*Int J Comput Assist Radiol Surg*. Author manuscript; available in PMC 2015 November 16.

Published in final edited form as:

*Int J Comput Assist Radiol Surg*. 2015 May ; 10(5): 665–676. doi:10.1007/s11548-014-1109-6.

## Wireless Mobile Technology to Improve Workflow and Feasibility of MR-Guided Percutaneous Interventions

Martin A. Rube, Dipl.-Ing. (FH)<sup>(1)</sup>, Andrew B. Holbrook, PhD<sup>(2)</sup>, Benjamin F. Cox, MD<sup>(1)</sup>, Razvan Buciu, MD<sup>(3)</sup>, and Andreas Melzer, MD, DDS<sup>(1)</sup>

<sup>(1)</sup>Institute for Medical Science and Technology, Division of Imaging and Technology, University of Dundee, Dundee, United Kingdom Wilson House, 1 Wurzburg Loan, DD2 1FD Dundee, United Kingdom

<sup>(2)</sup>Department of Radiology, Stanford University, Stanford, CA, United States 1201 Welch Rd, Stanford, CA 94305, United States

<sup>(3)</sup>Department of Radiology, Maimonides Medical Center, Brooklyn, NY, United States 4805 Fort Hamilton Parkway Brooklyn, NY 11219, United States

### Abstract

**Purpose**—A wireless interactive display and control device combined with a platform-independent web-based User Interface (UI) was developed to improve the workflow for interventional Magnetic Resonance Imaging (iMRI).

**Methods**—The iMRI-UI enables image acquisition of up to three independent slices using various pulse sequences with different contrast weighting. Pulse sequence, scan geometry and related parameters can be changed on the fly via the iMRI-UI using a tablet computer for improved lesion detection and interventional device targeting. The iMRI-UI was validated for core biopsies with a liver phantom (n=40) and Thiel soft-embalmed human cadavers (n=24) in a clinical 1.5T MRI scanner.

**Results**—The iMRI-UI components and setup were tested and found conditionally MRI-safe to use according to current ASTM standards. Despite minor temporary touchscreen interference at a close distance to the bore (<20 cm), no other issues regarding quality or imaging artefacts were observed. The 3D root-mean-square distance error was  $2.8 \pm 1.0$  (phantom) /  $2.9 \pm 0.8$  mm (cadaver) and overall procedure times ranged between 12–22 (phantom) / 20–55 minutes (cadaver).

---

Corresponding author: Martin Rube, Institute for Medical Science and Technology, University of Dundee, Wilson House, 1 Wurzburg Loan, DD2 1FD, Dundee, United Kingdom, Fax: +44 (0) 1382 386588; Phone: +44 (0) 1382 388355; m.rube@dundee.ac.uk.

#### **Ethical standards**

The human cadavers used in this study were donated according to standard procedures as set out in the Human Tissue (Scotland) Act 2006 and the Thiel Advisory Committee (University of Dundee, UK) has approved all our procedures.

#### **Conflict of interest**

The Integrated Interventional Imaging Operating System (IIOS) project has received funding from the European Community's Seventh Framework Programme (FP7/2007-2013) under Grant Agreement no 238802. Andrew B. Holbrook has received funding from the following grants NIH R01-CA121163 and P01-CA159992. Andreas Melzer is consultant and shareholder at INNOMEDIC GmbH, Herxheim, Germany.

**Conclusions**—The wireless iMRI-UI control setup enabled fast and accurate interventional biopsy needle placements along complex trajectories and improved the workflow for percutaneous interventions under MRI guidance in a preclinical trial.

### Keywords

magnetic resonance imaging (MRI); abdomen; image-guided liver intervention; MR remote control; mobile web technology; MRI-guided interventions

---

### Introduction

Percutaneous interventions under image guidance have become an important tool for diagnosis and treatment. In particular, Magnetic Resonance Imaging (MRI) can be valuable for guiding interventions where conventional X-Ray fluoroscopy, Computed Tomography (CT) or Ultrasound (US) cannot achieve the required detection of lesions [1–3] while avoiding potential risks of ionizing radiation [4] and nephrotoxic and allergenic iodine-based contrast agents [5]. MRI demonstrates superior soft-tissue contrast and native visualisation of blood vessels along with different contrast mechanisms for image acquisition. MRI provides true multi-planar imaging with arbitrary slice orientation and consequently allows to interactively align the scan plane according to an instrument trajectory [6] and target challenging lesions. Furthermore MRI can be utilised to assess lesions before, during and after a procedure [3].

Interventional MRI (iMRI) has been performed for more than two decades [7], but remains challenging for routine clinical practice [8] due to obstacles present in the MRI environment [9] (i.e. limited patient access, high acoustic noise and need for MRI-safe devices and equipment). Significant developments in the field of MRI have contributed to make scans faster [3, 10] and more efficient, and patient access has also significantly improved with modern open, short and wide bore systems [2, 11]. Nevertheless, various components and modifications are required for a conventional diagnostic MRI setup to enable iMRI [1]. To date, most scanner manufacturers provide moderately interactive real-time User Interfaces (UI) that are adequate for diagnostic MRI or available as work in progress packages [12, 13] for off label use only. In addition, a very limited number of display and input devices, such as tableside controls, are available allowing frequent dynamic changes to the scan acquisition and to date no simple means interaction with the MRI have been achieved.

A major source for complications and workflow delays is the need for leaving the scan room during interventions for viewing images and communicating with the radiographer. High acoustic noise levels during scanner operation, ranging between 70 and 110 dB [14], add a substantial health and safety risk, in particular, for fast gradient echo pulse sequences [14] that are frequently used for iMRI [3] applications. Hence, hearing protection is required as well as special creative solutions for audio communication [15] between interventionist, radiographer and patient. Guettler *et al.* proposed a wireless Bluetooth (BT)-based communication system that can be used during MRI scanner operation [16]. This concept was adopted for this study and extended for multiuser communication between physician, assisting staff and scanner operator using tablet personal computers (tablet PCs).

Wireless input devices such as tablet PCs are also promising candidates to be used at the patient side as interactive image display and for interactive MRI control. The display resolution of such tablet PCs is continuously improving such that modern tablet devices meet or exceed display resolution of desktop Liquid-Crystal Display (LCD) monitors in terms of dots per inch (DPI). The FDA has recently approved a tablet PC (iPad, Apple, Cupertino, CA, USA) and associated applications (apps) for radiologists to read diagnostic images. Recent studies have evaluated the image quality and diagnostic performance of tablet PCs in comparison to diagnostic LCD monitors for emergency brain CT scans [17] and for mobile on-call radiology in CT and MRI studies [18]. Holbrook *et al.* have proposed to use a tablet device for controlling or monitoring of an MRI-guided High Intensity Focused US (HIFU) procedures [19] and for collaborative iMRI [20].

Our objective was to improve percutaneous iMRI, through easy to use and inexpensive mobile tablet devices. Our implementation consisted of selected wireless tablet devices, a multi-user communication system and a platform independent web-based UI optimized for interactive iMRI. In comparison to the aforementioned real-time UIs provided by scanner manufacturers, our UI provides multi-touch functionality, which is crucial for tablet PCs i.e. to align scan planes, on the fly switching or interleaving of different MRI pulse sequences and enabling multiple devices to independently monitor and/or control the image acquisition.

This setup was validated for iMRI during percutaneous biopsies on gel phantoms and Thiel soft-embalmed cadaver experiments employing the MRI-guided freehand approach [2, 3, 6, 8, 11, 21].

## Materials and Methods

### iMRI Setup

The setup for validation is a dedicated imaging suite for MRI-guided interventions and surgery (see Fig. 1.) and consists of a clinical 1.5 T MRI scanner (Signa HDx, Software release 15.0M4A, GE Healthcare, Waukesha, WI, USA) connected to a surgical suite (1050, Maquet, Rastatt, Germany). A novel interventional coil suite (DuoFlex) developed in collaboration with MR Instruments Inc. (Minnetonka, MN, USA) and supported by GE Healthcare (Waukesha, WI, USA) was used for imaging. The DuoFlex coil suite facilitates access for interventional procedures with different combinations of coil elements. In this study, a 24cm 4-channel element was combined with a single loop coil with disposable cover (Fig. 3).

Two-way data communication between the MRI scanner (“MR Host”) and an external Linux (Ubuntu 11.10 64bit) workstation (16-CPU, 32 GB memory, z820, Hewlett-Packard, Palo Alto, CA) (“RT PC”) was accomplished via Gigabit Ethernet (IEEE 802.3z). In close proximity to the MRI unit, a 23-inch LCD monitor (SW2309W, Dell, Austin, TEX, USA) was installed on a flexible swivel arm. A second, shielded 40-inch LCD monitor (Mulleos 401, NEC Corporation, Tokyo, Japan) with the same resolution (1920 × 1080) was mounted to the opposite wall (Fig. 1). Note, ideally a second 40-inch LCD monitor should have been installed, which was not possible in our institution due to lack of space.

The integrity of galvanic isolation between the MRI control room and scan room was retained by using fibre-optic cables and optical-to-electrical as well as electrical-to-optical converters that keep Radio Frequency (RF) noise outside of the Faraday cage. Both monitors were connected with a fibre-optic cable (MI-1000, Opticis, Sungnam City, Korea) to the RT PC and used simultaneously to display the iMRI-UI. This allowed interventions to be performed from either side of the patient table with concomitant monitoring on the contralateral side on the 23 or 40-inch screen.

A Wireless Local Area Network (WLAN) was implemented for wireless data transfer within the scan room as illustrated in Fig. 1. The WLAN (2.4 GHz, IEEE 802.11) connection was established with a modified router (DIR615, D-Link, Taipei, Taiwan) where one antenna was positioned in the magnet room and the other one outside the Faraday cage providing the same local network Service Set Identifier (SSID) throughout both areas.

Interactive MRI pulse sequences with different contrast mechanisms were developed and implemented in the RTHawk software framework (Version 0.9.28, HeartVista, Inc., Palo Alto, CA, USA). RTHawk is a flexible research rtMRI software framework [22] and allows generation of new pulse sequences and dynamic changes to major aspects of data acquisition such as gradient waveforms, excitations and scan planes on the fly. Three interactive MRI pulse sequences were implemented that allow different contrast weightings ( $T_1$ ,  $T_2$ ,  $T_2/T_1$ ) for lesion detection and can be switched or interleaved on the fly. Sequences utilized included a Fast Spoiled Gradient Recalled echo sequence (FSPGR) that can provide rapid  $T_1$ -weighted imaging [23, 24], a balanced Steady State Free Precision (bSSFP) sequence for  $T_2/T_1$  contrast [25, 26] which was particularly useful for vessel visualisation by employing high flip-angles [27]. The third sequence is a reversed fast steady state precession (PSIF) sequence that is a time reversed variation of a Steady State Free Precision (SSFP) sequence providing fast  $T_2^*$ -weighted imaging for iMRI [28].

A dedicated multi-device iMRI-UI (Fig. 2) was developed and integrated into RTHawk. This UI allows scanner interaction through an Internet browser, across multiple operating systems and platforms such as PCs, tablet PCs or mobile phones [29]. MRI controls were integrated into a backend developed in C++. These were then attached to a locally hosted node.js server hosting the UI over a secure sockets layer (SSL), using a mongoDB database for authentication. The interface was developed exclusively with Hyper Text Markup Language (HTML), Cascading Style Sheets (CSS), and JavaScript, using the following open source libraries: Enyo 2.0 for the interface, Flot.js for plotting, and Three.js for HTML5 canvas and WebGL for rendering. The iMRI-UI was employed for image display, interactive scan and parameter control. It was designed to image up to three independent slices simultaneously. The UI also allowed the user to select different pulse sequences that can be interleaved and supports three-dimensional (3D) volume rendering of the slices. The iMRI-UI provides multi-touch functionality for touchscreen devices, on the fly adjustments for pulse sequence changes and scan geometry. Additional functions included windowing, annotations and bookmarking of scan planes and parameters (Fig. 2).

A Virtual Network Computing (VNC) connection was established between the MRI scanner running a VNC server and the MRI input device running a VNC client application to

compare the developed web UI to the standard real-time interface (GE i/Drive Pro Plus, GE Healthcare, Waukesha, WI), which is provided by the scanner manufacturer. The implemented web interface was also tested on various computers and mobile devices with different Internet browsers such as Mozilla Firefox (Ubuntu 11.10, OSX Snow Leopard), Google Chrome (Ubuntu 11.10, OSX Snow Leopard, MS Windows 7), and Apple Safari (OSX Snow Leopard) and Mobile Safari.

Subsequent to acceptance testing (MRI safety assessment according to ASTM F2052-06 [30] and evaluation of RF interference with a coherent noise (8ch HD brain coil, GRE, TE / TR= 13 / 32 ms, FOV = 20 cm × 20 cm, Matrix = 512×256, FA = 10°, Slice thickness = 5 mm, Bandwidth = 122.7 Hz/pixel) and a white pixel test (integrated body coil, Spin Echo EPI, TE / TR = 36.1 / 6000 ms, FOV = 9.9 cm × 9.9 cm, Matrix = 128×64, Slice thickness = 10 mm, Bandwidth = 3906.25 Hz/pixel) protocol), two mobile tablet PCs have been selected (iPad 1 and 3, Apple, Cupertino, US) with a 9.7 inch (diagonal) multi-touch display and a resolution of 1024×768 and 2048 × 1536 pixels respectively. During interventions one tablet was solely used for communication (iPad 1) and the other one for MRI display and control. Each tablet PC was inserted into a plastic cover to simulate sterile equipment and mounted to a customized MRI-safe intravascular pole (GE Healthcare, Waukesha, WI, USA) with modified car mounts for tablet devices (Matek Trading Co., Ltd, Hanoi, Vietnam). Note, a comprehensive assessment of various mobile input and control devices that can be used for MRI operations along with various options for wireless data communication will be published elsewhere.

Two-way communication between the scanner operator, the physician, and the assisting nurse was established using Voice-over-Internet-Protocol (VoIP) technology and wireless mobile BT headsets (Calisto B70, Plantronics, Santa Cruz, CA, USA) integrated into modified earmuffs (RS Components Ltd, Corby, UK). Two-way communication was also established with two tablet PCs in the scan room and a PC in the control room using a VoIP software application (Skype, Luxembourg City, Luxembourg).

### Techniques for MRI-guided Interventions

An experienced interventional radiologist (10 years experience – “expert”) and one physician in training (no interventional experience – “novice”) performed all procedures. A carbon fibre composite (CFK) puncture needle with Nitinol mandrin (21G / 150 mm, Radimed, Bochum, Germany) was used during MRI-guided needle punctures. Tissue samples (in case of artificial targets) were obtained for verification with an MRI-safe biopsy needle (MR Biopsy-Handy, 16G, 15cm, Somatex, Teltow, Germany). Passive, susceptibility-based visualisation of the needles [31, 32] was applied for needle guidance.

Initially, a planning dataset with high spatial resolution (FSPGR, TE / TR = 10 / 80 ms, FA = 60, FOV = 25 cm × 25 cm, Matrix = 384×384, Slice thickness = 2 mm) was acquired and the target and skin entry points were selected. The target point was defined as a sphere with 8 mm diameter. The patient table was then moved out of the bore and the physical entry point was marked on the skin/surface by calculating the distance offset from the laser crosshair. A small incision was then performed using a non-magnetic scalpel at the entry point and the needle was positioned. The patient table was then moved back into the MRI

scanner while the physician kept his finger at the skin entry point to mark-up the location on the subsequent MRI images. The scan acquisition was then initiated and once the physician was satisfied with the location of the skin entry point, the needle was inserted under rtMRI guidance with the pulse sequence and parameter selection of the physician (bSSFP, FSPGR, PSIF). MR fluoroscopy was terminated when the needle was positioned in the lesion. A second high-resolution dataset (the same sequence and parameters as during planning) was then acquired with the needle still in place to verify the needle position. Note, the imaging pulse sequences and parameters were optimized for MRI of Thiel soft-embalmed cadavers [33].

An intervention was rated successful if the needle tip was positioned within the predefined target region and clearly identified on multiple rt-MRI planes and in the high-resolution dataset. In the case of targeting Gd-doped target visual checks were additionally conducted to ensure that the desired targeting was achieved. The root-mean-square (RMS) 3D error was calculated based on the high-resolution dataset for the discrepancy between the actual needle tip and the target point position (3D coordinates of the planned target point). Analysis of variance (ANOVA) was used ( $p=0.05$ ) to test the level of experience of the clinician on targeting accuracy. A post-hoc test was performed to test statistical significance between the group of participants and between experiments.

### **In Vitro Phantom Experiments**

The in vitro experiments were conducted in a muscle tissue-mimicking, ballistic gelatine phantom with 10% w/w gelatine powder (G8-500, Fisher Scientific, Hampton, NH, USA) [34]. A range of targets (diameter 20 mm), mimicking lesions and consisting of gelatine, agar (A360-500, Fisher Scientific, Hampton, NH, USA), fat and food colouring (Dr. Oetker, Bielefeld, Germany) for visual confirmation were positioned within the gelatine matrix. A layer of boiled spaghetti (Buitoni, Sansepolcro, Italy) in gelatine was added to the phantom to mimic blood vessels that should be avoided during targeting.

Each physician performed ten double (trajectory lengths ranged from 80 – 160 mm) and ten single oblique interventions (trajectory lengths ranged from 100 – 160 mm). The times for needle targeting and the total intervention were recorded.

### **Ex Vivo Experiments Using Thiel Soft-Embalmed Human Cadavers**

Thiel [35] proposed a soft-embalming technique that sustains tissue flexibility, colouring and integrity. The human cadavers used in this study were donated according to standard procedures as set out in the Human Tissue (Scotland) Act 2006 and the Thiel Advisory Committee (University of Dundee, UK) has approved all our procedures. Thiel embalmed cadavers with re-established mechanical ventilation with associated organ motion and partially vascular re-perfusion have been developed in Dundee for iMRI research and training [33, 36–38]. These cadavers represent anatomically correct models complete with anatomical variances [36] and were found suitable for MRI [33]. However, MRI of Thiel soft-embalmed cadavers is constrained by limited RF penetration and gradient echo based sequences have been shown to generate better MR images than spin-echo based pulse sequences [33].

Three Thiel soft-embalmed cadavers (sex: 1 female and 2 male, age: 50 – 75 years, weight: 65 – 80 kg) were prepared in the angio suite (the room on the left side in Fig. 1) and then transferred to the MRI suite (Fig. 3). The peripheral cannulation and tumour phantom implant was performed through a pre-existing median laparotomy. Gadolinium (Gd) doped targets (agar/fat, 25 mm diameter) were implanted to mimic liver lesions that appear bright in T<sub>1</sub>-weighted images for targeting. Alternatively target choice was predetermined during the procedure planning stages on a MR distinctive area within the liver parenchyma (one cadaver).

An MRI compatible anaesthetic ventilator (ventiPAC, PneuPAC Ltd., Luton, UK) was used for mechanical ventilation (Inspiration time T<sub>I</sub> = 2 s, Expiration time T<sub>E</sub> = 4 s, and tidal volume V<sub>T</sub> = 750 ml) with tracheal intubation to simulate hepatic motion throughout the procedure. The expert and the novice performed four double oblique interventions (trajectory lengths ranged from 60 – 120 mm) in each human cadaver.

## Results

The tablet devices (Fig. 4) that were used in this study can be operated with gloves while covered in sterile drapes as illustrated in Fig. 4c. According to the standard test method [30], the tablet PC experienced a magnetically induced displacement force of 4.90 N at the location of maximum deflection (mean deflection angle of 34°). No displacement force was present for the tablet PC at a distance greater or equal to 50 cm (4–10 mT) from the end of the bore.

Audio communication via VoIP was possible throughout all interventions with a stable BT connection. However, during scanner operation the acoustic noise level was high, which led to imperfect sound quality, but was rated suitable for communication.

No degraded image quality or RF interference could be detected on any MR image, the white pixel, or on a coherent noise test while the devices were set up in the scan room and the WLAN connection was established. In particular no additional frequencies were found in the bandwidth of the receiver, the SNR measurements were not more than 10 % lower than the reference measurements, which did not alter images significantly nor render images non-diagnostic.

The WLAN supplied by the modified router provided a stable and fast connection, facilitating rapid image update rates without noticeable delay for the rtMRI feed into the scan room. Using the VNC connection provided a feasible connection with the scanner manufacturers UI but the performing physicians rated the latency (ranging between 0.2 – 1.3 seconds) between actual image acquisition and display unacceptable for performing interventions. On the contrary, the node.js server showed no noticeable acquisition lags or time delays displaying images to the clients (Fig. 4c). Multiple connections were established (i.e. via multiple browsers on one PC and across several tablet devices), with all able to access and visualize (monitoring) the data individually or controlling the procedure per login permissions.

## In Vitro Phantom Validation

All phantom biopsies ( $n = 40$ ) were technically successful (needle tip was positioned within the predefined target region). The mean RMS 3D error between the planned target point and the needle tip was  $2.8 \pm 1.0$  mm, with further details given in Table 1. The mean targeting time was 5 minutes and 21 seconds and the mean procedure time was 15 minutes and 46 seconds (range 10 – 19 minutes) for the expert. The mean targeting time was 6 minutes and 35 seconds and the mean procedure time was 17 minutes and 31 seconds (range 12 – 22 minutes) for the novice.

Our in-room interactive tablet PCs provided the operator with images in near real-time and the ability to self-select important parameters or switch between pulse sequences on the fly (one click on the touch screen and with no delay). Parameter control and slice repositioning from inside the scan room was achieved, facilitating fast navigation to the target. The close proximity of the touch device allowed for zooming (Fig. 4c and d) and precise target acquisition during simulated interventions (Fig. 5). The interventional workflow for a freehand needle biopsy illustrated in Fig. 5a – d. The web UI displayed three different slices (Fig. 5e) that were updated on the tablet PC while a needle biopsy was performed with a single oblique trajectory.

## Thiel Human Cadaver Experiments

All cadaver biopsies ( $n = 24$ ) were technically successful (needle tip was positioned within the predefined target region) under simulated free breathing conditions. The mean RMS 3D error between the planned target point and the needle tip was  $2.9 \pm 0.8$  mm for the expert and  $4.1 \pm 0.9$  mm for the novice, with further details given in Table 1. The variations between individual cadavers (surgical history, post mortem training procedures, the shelf time, pre-existing or artificial lesions) were found to be significant. Detailed recording of procedure times (ranging from 20 – 55 minutes) was abandoned for the Thiel soft-embalmed cadaver experiments due to the influence of confounding variations and problems inherent with cadaver models, which are not present in living patients. These include trapped air (green arrow in Fig. 6e) in the abdominal cavity, decreased liver dimensions due to dehydration, lower quality of tissue in general, and pre-existing damage due to previous surgical training events.

A screenshot of a successful needle puncture with a double oblique trajectory is shown in Fig. 6 and Fig. 7. The screenshot of the web UI (Fig. 6d) contains three near real-time MR images that are frequently updated with a  $T_1$  weighted pulse sequence in three different slice orientations. The needle was advanced during continuous MRI with a temporal resolution of 1 frame per second. A correct needle placement was then confirmed with the high spatial resolution dataset (Fig. 8). Trapped air (green arrow in Fig. 6e) in the abdominal cavity of the cadaver, decreased liver dimensions (compared to a liver in a living human) and a short needle that was required for the 60 cm bore diameter constrained the choice of potential needle paths.

ANOVA showed significant difference between the participants and between experiments. However, when considering the interaction effect, ANOVA indicated no significant

difference. The post-hoc test showed no significant difference between the double oblique approaches in the phantom and the Thiel cadavers. But it showed significant difference between the single oblique and double oblique approach (both in the phantom and Thiel cadavers).

## Discussion

A substantial hurdle for clinical acceptance of MRI-guided percutaneous interventions is the lack of a dedicated and efficient workflow [8] that is required for effective procedures in the complex MR environment. We have therefore developed and validated a wireless system for communication and interactive remote control of a clinical whole body MRI scanner to facilitate iMRI.

Our setup was implemented on a research scanner and therefore it was permitted to incorporate components that are currently not approved for clinical use. However, wireless mobile tablet PCs can be applied with little effort and used for scanner remote control as well as communication during iMRI. Commercialization of the Bluetooth communication and the wireless interactive display and control device is currently being investigated.

The magnetically induced deflection angle was measured to be less than  $45^\circ$ , which means a deflection force induced by the field of the 1.5 T MRI scanner is less than the force on the device due to gravity [30]. While these results are a good indication for MRI safety, the test method for magnetically induced displacement force alone is not sufficient for ultimately determining the device safety in the MRI environment and further testing may be required before clinical application [30] and regulatory approval. The authors therefore advise caution in reproducing the described setup and each solution should be approved by the local MRI safety authorities and tested individually.

### Interventional MRI Workflow

One of the challenging but important technical tasks during MRI-guided needle interventions regard selecting the correct MRI scan planes and maintaining an appropriate angulation during needle placement [39]. Slice re-alignments typically require significant intra-procedure communication [8] and time. The close proximity of the touch screen improved the scanner interaction considerably during phantom and cadaver experiments respectively.

A VNC connection provides multiple users access to centralized high performance resources. We evaluated this option for remote control of our MRI scanner via conventional or consumer devices [40]. Although, our results demonstrate that the latency for the imaging feed was unacceptable for iMRI. In comparison to our setup, the standard commercially available real-time UI that was available on our scanner (i/Drive Plus, GE Healthcare, Waukesha, WI, USA) provided only limited features and can only be used with a single pulse sequence (FGRE – RF spoiled or unspoiled) and one interactive imaging plane at a time. The proposed web UI allowed flexible and intuitive scan plane adjustments in real-time. Different contrast mechanisms ( $T_1$ ,  $T_2$ ,  $T_2/T_1$ ) can interactively be selected on the fly and also be interleaved. The availability of various contrast mechanisms is particularly

useful as opposed to a sequence with only a single contrast weighting, which may not generate satisfactory contrast among pathologic and normal tissue, which compromises lesion assessment and MRI guidance [28].

The device trajectory could be adjusted dynamically in the course a procedure and decreased needle passage that is associated with trauma and bleeding and causes workflow interruptions [6, 8]. Up to three real-time imaging planes could be selected and were frequently updated according to the user selected parameter and pulse sequence choice. It should be noted that the three planes were a design choice based on user feedback and not a capability limitation.

Our interventional radiologists concluded that our setup resembles a suitable hybrid approach combining the workflow from CT with real-time needle guidance capability encountered with ultrasound coupled with the superior soft tissue contrast of MRI [41]. The proposed image guidance arrangements were also found satisfactory in terms of decreasing procedure interruptions such as moving clinical staff in and out of the scan room, moving the patient in and out of the bore as well as scan interruptions for sequence and parameter updates.

The established multi-user communication with a wireless setup can be potentially produced at a relatively low cost (the cost of our additional components was approximately \$3000) and clearly improved our iMRI workflow compared to previous experiments. This benefit must be quantified in further controlled studies. Additional acoustic or digital noise filtering has the potential to enhance the communications [16]. It should be noted that we decided to use Skype for our experiments, as it was freeware and compatible with all operating systems (Linux, Mac OS, Windows) that were used. For experiments involving patients other software solutions are required that firstly, provide security and safety of patient information and secondly, will be able to work in a clinical environment with secure local networks. The commercially available communication software Lync (Microsoft, Redmond, WA, USA) could be one potential solution, which is currently being investigated for internal communication in multiple hospitals.

Controlling an MRI scanner and guiding interventional procedures from a web browser presents many interesting solutions for device integration. The web-based model allows easy access to data and the experimental controls, whether in close proximity to the scanner or remotely located. This could enable an intuitive and collaborative multi-user approach for MRI-guided interventions, and facilitate educational demonstrations or collaborative treatment planning. Theoretically, MRI-guided interventions, including thermal treatments, could be assisted and monitored remotely. However, there is a potential issue with latency and procedural safety when factoring in distance and network traffic that may not be encountered with a LAN.

At present MRI system software architecture is still domain of the main scanner manufacturers. Regulatory hurdles and proprietary rights make any expansion or custom adaptation to the pulse sequence environment difficult. In principle our webUI can operate on top of any platform but would require a means of communicating with the MRI scanner

and thus the MRI scanner manufacturers have to grant access to main functions of their software architecture. In our case the implementation was implemented on top of RTHawk, which is currently limited to GE scanners and has not received regulatory approval.

### Phantom and Thiel Human Cadaver Validation

All experiments in this study were performed in a closed bore MRI scanner with 60 cm bore diameter. This limited the selection of individual cadavers and the choice of needle trajectories and the achievable target depth because only short needles could be used in the narrow bore. A short and wide bore scanner could significantly improve patient access and device placements [3, 6, 8, 11]. It should be noted that our scanner control via mobile tablet PCs in combination with auto-land marking [42] could furthermore facilitate interventions on the other side of the bore where patients might be more accessible (no patient table mount) but generally no MRI controls are located at this position (i.e. current wide bore MRI scanner models). Targeting accuracy is essential for image-guided interventions and an in-plane error of 5 mm is acceptable in most clinical situations according to Rothgang and colleagues [8]. The 3D error (RMS) was found to be below this value in the phantom and the cadaver experiments performed by the expert and novice. Our targeting accuracy results (Table 1) are equivalent to the targeting errors that have previously been reported (Stattaus et al. [11] - in vivo: 3.4 mm median lateral deviation, Fischer et al. [21] – 5.2 mm mean in-plane error, Rothgang et al. [8] - phantom / in vivo: 1.8 mm / 2.9 mm mean targeting error in all directions) for MRI-guided percutaneous interventions employing the freehand technique. The mean puncture times (novice: 6 minutes and 35 seconds / expert: 5 minutes and 21 seconds) and mean procedure times (novice: 17 minutes and 31 seconds / expert: 15 minutes and 46 seconds) are reasonable in comparison to what previous freehand liver biopsy studies have reported (Stattaus et al. [11] - in vivo: 19 minutes mean puncture time, Das et al. [1] – in vivo: 20 - 25 minutes mean intervention time, Fischbach et al. [10] – in vivo: 18 minutes mean intervention time). The variation between individual cadavers, i.e. time of death to embalming, the shelf time, the surgical history (causing air trapped within the abdominal and thoracic cavities, displaced and shrunken liver, lack of blood supply and unusual liver motion), which affects the MRI properties [33], and whether or not pre-existing (one cadaver) or artificial lesions were employed, influenced procedure times. Our cadavers were also used in previous training procedures, which affected usability in particular due to preformed incisions and trapped air. Due to the influence of these cadaver specific variations, which are not found during clinical procedures, detailed recording of procedure times was not applied during the Thiel soft-embalmed cadaver experiments. Further experience with the cadaver model, vascular reperfusion [43] and adaptation of technique should solve many of these problems so that the benefit of the real human anatomy [36] can be fully explored for the development and training of iMRI procedures.

In conclusion, MRI has unique potential for guiding percutaneous interventions specifically for procedures that cannot be performed safely or satisfactorily using other guidance modalities due to lack of tissue contrast, imaging interference (e.g. ribs or air filled bowel during US) [3], vascular imaging [3] or ionising radiation [4], which is most relevant e.g. for young patients [2]. However, percutaneous interventions under MRI guidance are not yet clinically accepted procedures. Workflow improvements are essential [8] in an environment

with high system and procedure complexity. The presented components and techniques improve percutaneous interventions under MRI guidance by providing interactive and intuitive MRI acquisition control as well as scanner operator – physician – assistant communication. By creating a dual room WLAN and platform independent applications capable of interacting with the MRI scanner and potentially other important devices in the scan room, cost effective, versatile and intuitive means for improving workflow for iMRI have been demonstrated in preclinical experiments.

## Acknowledgments

The authors thank Joelle Barral, William Overall and Juan Santos (HeartVista, Inc., Palo Alto, CA, USA) for technical support and Fabiola Fernandez-Gutierrez for her support in statistical analysis. Special thanks also to John Ferut (GE Healthcare, Waukesha, WI), Tom Breslin and Gabor Mizsei (MR Instruments Inc., Minnetonka, MN, USA) for valuable input and kind support. The authors are thankful for financial assistance provided by the FUSIMO (“Patient specific modeling and simulation of focused ultrasound in moving organs”) project funded under the European Community’s Seventh Framework Programme (FP7/2007-2013) for Research and Technological Development under Grant Agreement no 270186. The Marie Curie Initial Training Network - Integrated Interventional Imaging Operating System (IIIOS) funded the authors Martin A. Rube, Benjamin F. Cox, Andrew B. Holbrook and R. Buciu and supported this work. The IIIOS project has received funding from the European Community’s Seventh Framework Programme (FP7/2007-2013) under Grant Agreement no 238802. The authors also acknowledge the funding sources NIH R01-CA121163 and P01-CA159992.

## References

1. Das CJ, Goenka AH, Srivastava DN. MR-guided abdominal biopsy using a 1.5-Tesla closed system: a feasibility study. *Abdom Imaging*. 2009; 35:218–23. [PubMed: 19259724]
2. Hoffmann R, Thomas C, Rempp H, Schmidt D, Pereira PL, Claussen CD, Clasen S. Performing MR-guided biopsies in clinical routine: factors that influence accuracy and procedure time. *Eur Radiol*. 2012; 22(3):663–71. [PubMed: 21960160]
3. Weiss CR, Nour SG, Lewin JS. MR-guided biopsy: a review of current techniques and applications. *J Magn Reson Imaging*. 2008; 27(2):311–25. [PubMed: 18219685]
4. Mathews JD, Forsythe aV, Brady Z, Butler MW, Goergen SK, Byrnes GB, Giles GG, Wallace aB, Anderson PR, Guiver Ta, et al. Cancer risk in 680 000 people exposed to computed tomography scans in childhood or adolescence: data linkage study of 11 million Australians. *BMJ*. 2013; 346:f2360. [PubMed: 23694687]
5. Bartorelli AL, Marenzi G. Contrast-induced nephropathy. *J Interv Cardiol*. 2008; 21(1):74–85. [PubMed: 18086132]
6. Moche M, Trampel R, Kahn T, Busse H. Navigation concepts for MR image-guided interventions. *J Magn Reson Imaging*. 2008; 27(2):276–91. [PubMed: 18219682]
7. Mueller P, Stark D, Simeone F, Saini S, Butch R, Edelman RR, Wittenberg J, Ferrucci JT. MR-guided aspiration biopsy: needle design and clinical trials. *Radiology*. 1986; 161:605–9. [PubMed: 3786706]
8. Rothgang E, Gilson WD, Wacker F, Hornegger J, Lorenz CH, Weiss CR. Rapid freehand MR-guided percutaneous needle interventions: An image-based approach to improve workflow and feasibility. *J Magn Reson Imaging*. 2013; 37(5):1202–12. [PubMed: 23334924]
9. Jolesz FA, Morrison PR, Koran SJ, Kelley RJ, Hushek SG, Newman RW, Fried MP, Melzer A, Seibel RM, Jalahej H. Compatible instrumentation for intraoperative MRI: expanding resources. *J Magn Reson Imaging*. 1998; 8(1):8–11. [PubMed: 9500254]
10. Fischbach F, Bunke J, Thormann M, Gaffke G, Jungnickel K, Smink J, Ricke J. MR-guided freehand biopsy of liver lesions with fast continuous imaging using a 1.0-T open MRI scanner: experience in 50 patients. *Cardiovasc Intervent Radiol*. 2011; 34(1):188–92. [PubMed: 20358370]
11. Stattaus J, Maderwald S, Forsting M, Barkhausen J, Ladd ME. MR-Guided core biopsy with MR fluoroscopy using a short, wide-bore 1.5-Tesla scanner: Feasibility and initial results. *J Magn Reson Imaging*. 2008; 27:1181–7. [PubMed: 18425833]

12. Lorenz, CH.; Kirchberg, KJ.; Zuehlsdorff, S.; Speier, P.; Caylus, M.; Borys, W.; Moeller, T.; Guttman, MA. Interactive Frontend (IFE): A platform for graphical MR scanner control and scan automation. Proc. Intl. Soc. Mag. Reson. Med. 13; Miami, FL, USA. 2005. p. 2170
13. Smink J, Haaekkinen M, Holthuizen R, Krueger S, Ries M, Berber Y, Moonen C, Köhler M, Vahala E. eXTernal Control (XTC): a flexible, real-time, low-latency, bi-directional scanner interface. Proc Intl Soc Mag Reson Med. 2011; 20:1755.
14. McJury M, Shellock FG. Auditory noise associated with MR procedures: a review. J Magn Reson Imaging. 2000; 12(1):37–45. [PubMed: 10931563]
15. Ratnayaka K, Faranesh AZ, Guttman MA, Kocaturk O, Saikus CE, Lederman RJ. Interventional cardiovascular magnetic resonance: still tantalizing. J Cardiovasc Magn Reson. 2008; 10(1):62–85. [PubMed: 19114017]
16. Guettler, FV.; Rump, JC.; Teichgraeber, U. MR-compatible wireless communication system for the interventional open high-field MRI. Proc. Intl. Soc. Mag. Reson. Med; Honolulu, HI, USA. 2009. p. 2576
17. Mc Laughlin P, Neill SO, Fanning N, Mc Garrigle AM, Connor OJO, Wyse G, Maher MM. Emergency CT brain: preliminary interpretation with a tablet device: image quality and diagnostic performance of the Apple iPad. Emergency Radiology. 2011; 19(2):127–33. [PubMed: 22173819]
18. John S, Poh ACC, Lim TCC, Chan EHY, Chong LR. The iPad tablet computer for mobile on-call radiology diagnosis? Auditing discrepancy in CT and MRI reporting. J Digit Imaging. 2012; 25(5):628–34. [PubMed: 22562174]
19. Holbrook, AB.; Watkins, RD.; Pauly, KB. Interactive interventional applications for the MRI scan room. Proc. Intl. Soc. Mag. Reson. Med; Melbourne, Australia. 2012. p. 2954
20. Holbrook, AB.; Butts Pauly, K. Collaborative MRI for improving patient throughput. Proc. Intl. Soc. Mag. Reson. Med; Melbourne, Australia. 2012. p. 2956
21. Fischer GS, Deguet A, Csoma C, Taylor RH, Fayad L, Carrino JA, Zinreich SJ, Fichtinger G. MRI image overlay: application to arthrography needle insertion. Comput Aided Surg. 2007; 12(1):2–14. [PubMed: 17364654]
22. Santos, JM.; Wright, Ga; Pauly, JM. Flexible real-time magnetic resonance imaging framework. Conf Proc IEEE Eng Med Biol Soc; San Francisco, CA, USA. 2004. p. 1048-51.
23. Haase A, Frahm J, Matthaei D, Haenike W, Merboldt KD. FLASH Imaging. Rapid NMR Imaging Using Low Flip-Angle Pulses. J Magn Reson. 1986; 67(2):258–66.
24. Zur Y, Wood ML, Neuringer LJ. Spoiling of transverse magnetization in steady-state sequences. Magn Reson Med. 1991; 21(2):251–263. [PubMed: 1745124]
25. Oppelt A, Graumann R, Barfuß H, Fischer H, Hartl W, Schajor W. FISP: eine neue schnelle pulssequenz fuer die kernspintomographie. Electromedica. 1986; 54:15–8.
26. Deimling, M.; Heid, O. Magnetization prepared true FISP imaging. Proc. Intl. Soc. Mag. Reson. Med; San Francisco, CA, USA. 1994. p. 495
27. Duerk JL, Lewin JS, Wendt M, Petersilge C. Remember true FISP? A high SNR, near 1-second imaging method for T2-like contrast in interventional MRI at .2 T. J Magn Reson Imaging. 1998; 8(1):203–8. [PubMed: 9500281]
28. Chung YC, Merkle EM, Lewin JS, Shonk JR, Duerk JL. Fast T2-weighted imaging by PSIF at 0.2 T for interventional MRI. Magn Reson Med. 1999; 42(2):335–44. [PubMed: 10440959]
29. Holbrook, AB.; Rube, MA.; Melzer, A.; Butts Pauly, K. In: Kapur, T.; Jolesz, FA.; Lewin, J.; Kahn, T., editors. Interventional MRI from the Internet Browser; Proceedings of the 9th Inteventional MRI Symposium; Boston, MA, USA. 2012. p. 114
30. ASTM International. F2052-06: Standard test method for measurement of magnetically induced displacement force on medical devices in the magnetic resonance environment. 2006.
31. Ladd ME, Erhart P, Debatin JF, Romanowski BJ, Boesiger P, McKinnon GC. Biopsy needle susceptibility artifacts. Magn Reson Med. 1996; 36(4):646–51. [PubMed: 8892221]
32. Melzer, Michitsch, Konak, Schaefer, Bertsch T. Nitinol in magnetic resonance imaging. Minim Invasive Ther Allied Technol. 2004; 13(4):261–71. [PubMed: 16754135]
33. Gueorguieva MJ, Yeo DTB, Eisma R, Melzer A. MRI of Thiel-embalmed human cadavers. J Magn Reson Imaging. 2013 Epub ahead of print. 10.1002/jmri.24210

34. Jussila J. Preparing ballistic gelatine--review and proposal for a standard method. *Forensic Sci Int.* 2004; 141(2–3):91–8. [PubMed: 15062946]
35. Thiel W. Eine Arterienmasse zur Nachinjektion bei der Konservierung ganzer Leichen. [An arterial substance for subsequent injection during the preservation of the whole corpse]. *Ann Anat.* 1992; 174:197–200. [PubMed: 1503237]
36. Cox BF, McLeod H, Rube M, Vinnicombe S, Holbrook B, Eisma R, Saliev T, Karakitsios I, Melzer A. MR real-time tracking of hepatic motion during respiration in a Thiel Soft-fix cadaver. *Biomed Tech.* 2012; 57:4399.
37. Eisma R, Lamb C, Soames RW. From formalin to thiel embalming: What changes? One anatomy department's experiences. *Clin Anat.* 2013; 26(5):564–71. [PubMed: 23408386]
38. Eisma R, Gueorguieva M, Immel E, Toomey R, McLeod G, Soames R, Melzer A. Liver displacement during ventilation in Thiel embalmed human cadavers - a possible model for research and training in minimally invasive therapies. *Minim Invasive Ther Allied Technol.* 2013 Epub ahead of print. 10.3109/13645706.2013.7
39. Sakarya ME, Unal O, Ozbay B, Uzun K, Kati I, Ozen S, Etlik O. MR fluoroscopy-guided transthoracic fine-needle aspiration biopsy: feasibility. *Radiology.* 2003; 228(2):589–92. [PubMed: 12819336]
40. Richardson T, Stafford-Fraser Q, Wood KR, Hopper A. Virtual network computing. *IEEE Internet Computing.* 1998; 2(1):33–8.
41. Gedroyc WM. Interventional magnetic resonance imaging. *BJU international.* 2000; 86(Suppl 1): 174–80. [PubMed: 10961287]
42. Hancu, I.; Park, K.; Darrow, R. A landmark-free MRI scanner concept. *Proc. Intl. Soc. Mag. Reson. Med; Melbourne, Australia.* 2012. p. 2744
43. Cox, BF.; Eisma, R.; Rube, MA.; Gueorguieva, M.; McLeod, H.; Immel, E.; Melzer, A. Developing Thiel soft-fix cadavers as a suitable model for iMRI training and research. *Proceedings of the 9th Interventional MRI Symposium; Boston, MA, USA.* 2012. p. 103
44. Adam G, Buecker A, Tacke J, Guenther RW. Interventional MR imaging: percutaneous abdominal and skeletal biopsies and drainages of the abdomen. *Eur Radiol.* 1999; 9(8):1471–8. [PubMed: 10525854]

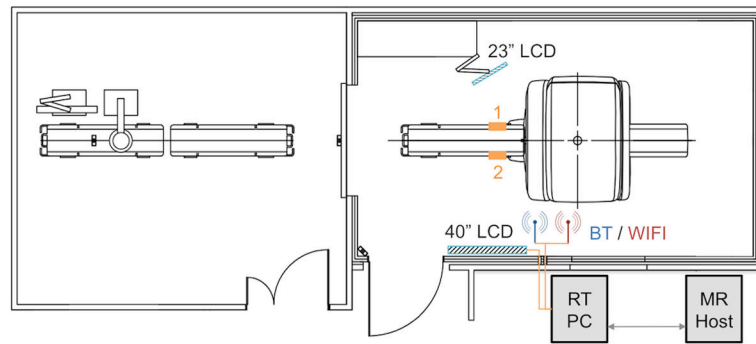


**Fig. 1.** 2D floor plan with wireless control and communication setup – 1 and 2 represent the mounting positions of the control and input devices. The position can be changed according to the preference of the physician in terms performing interventions from the left or the right side of the patient table or on the other side of the bore

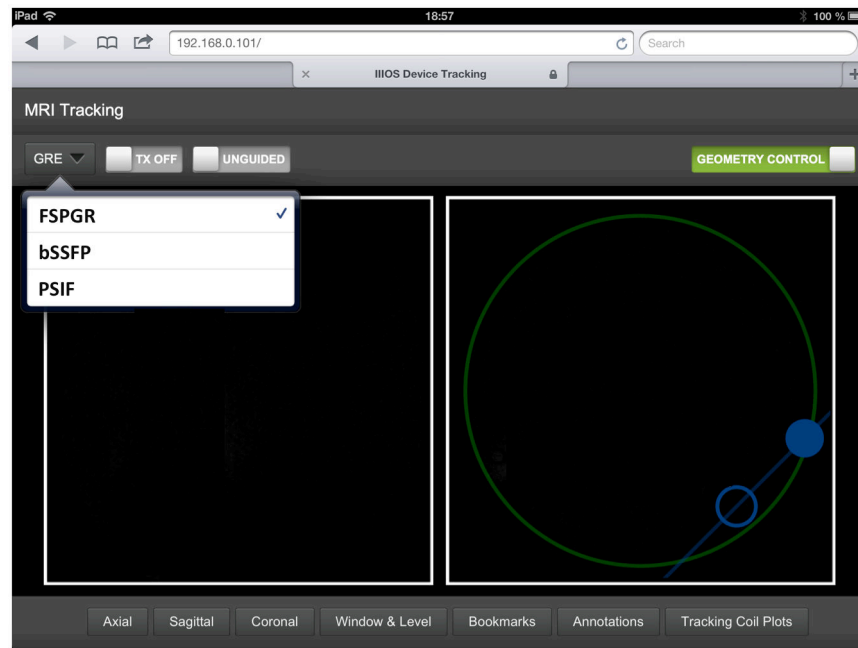


**Fig. 2.**

Screenshot of the web-based user interface for iMRI running on a tablet PC - Two imaging planes are shown exemplarily. Up to three real-time imaging planes can be selected that are frequently updated according to the user-selected geometry, scan parameter and pulse sequence choice. The pulse sequence can be selected from dropdown list located on the top left corner of the screen under the browser address bar. The geometry control can be activated next to the pulse sequence drop down menu and the scan plane orientation can be adjusted with multi-touch gestures using the interactive geometry tool (green line with dot) or set to standard radiologic views (axial, sagittal, coronal). Other features of the user interface include windowing, annotations and bookmarking of scan planes and parameters.



**Fig. 3.** Photograph of a Thiel soft-embalmed human cadaver positioned in front of the MRI scanner. The single loop element is positioned anterior for good percutaneous access to the liver while the 4-channel paddle element of the DuoFlex interventional coil is positioned posterior. The black strap is used for compression of the chest to improve hepatic access

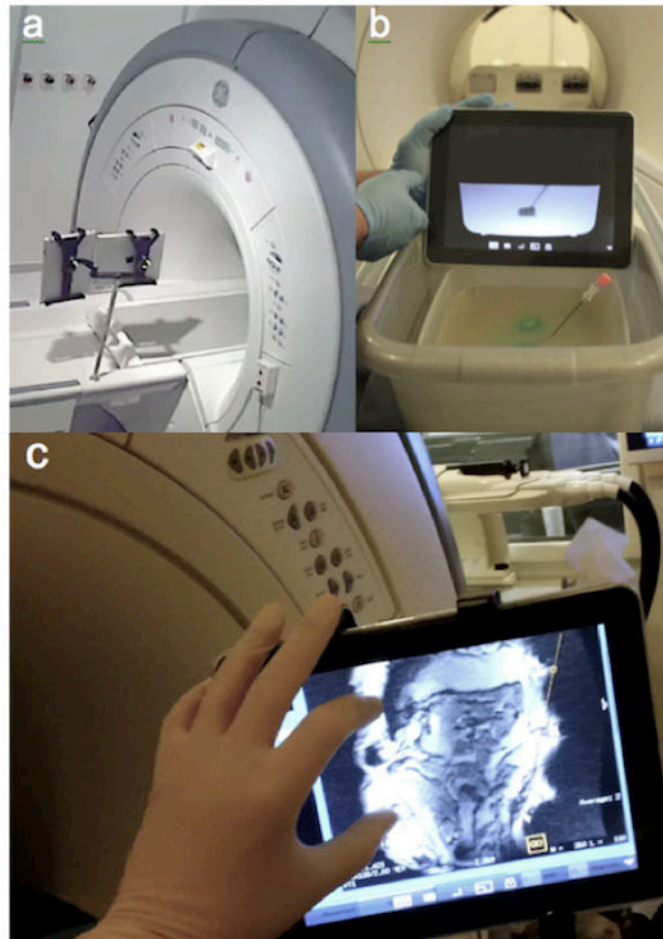


**Fig. 4.**

Wireless scanner interaction from within the magnet room with the tablet device. The multi-touch mobile tablet PCs are mounted on an MRI compatible intravascular pole (a), whereas, one tablet is used to display the iMRI-UI while the other tablet is used for communication in combination with the BT headsets. A successful needle puncture is demonstrated (b) in the phantom. The physician (wearing gloves) is also able to zoom into relevant details on the tablet PC as illustrated during a needle biopsy in a Thiel embalmed human cadaver (c)

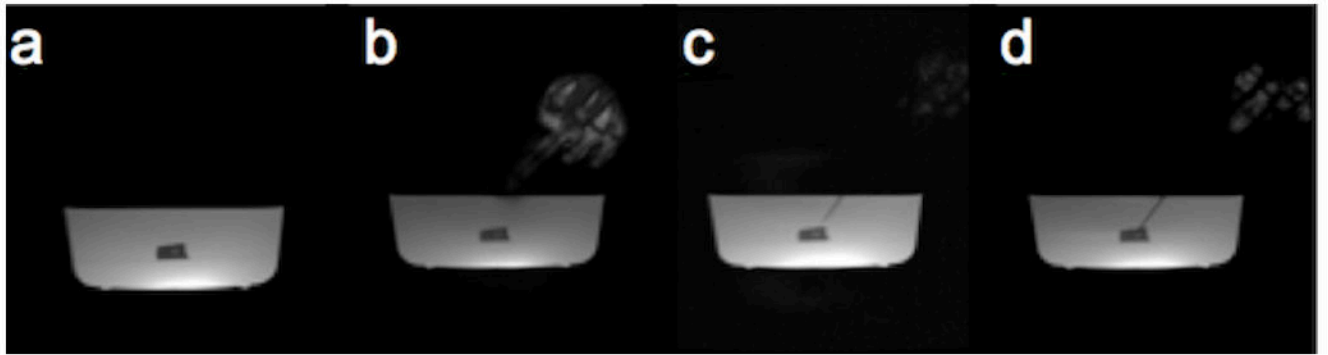


**Fig. 5.** Simplified freehand needle biopsy for a single oblique trajectory under near real-time MRI guidance (FSPGR, TE/TR = 4.0 / 8.3 ms, Matrix =  $256 \times 256$ , FOV = 33 cm  $\times$  33 cm, FA =  $60^\circ$ , Slice thickness = 7 mm). The target lesion is shown in (a). The needle entry point is identified (b) by finger pointing (44) and the real-time scan plane is then updated to contain the skin entry and target point. The needle is then advanced towards the intended target (c) and the lesion is punctured (d). A screenshot is acquired on the tablet PC illustrating the puncture step during the freehand needle biopsy for a double oblique trajectory

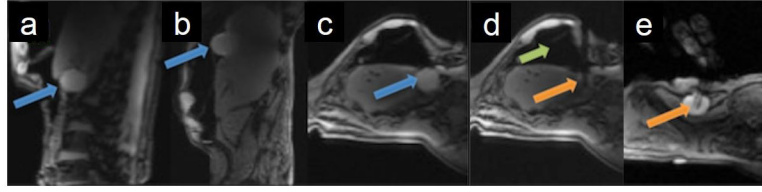


**Fig. 6.**

MRI-guided liver biopsy in a Thiel embalmed human cadaver performed with the freehand technique and under simulated free-breathing conditions. The implanted targets (blue arrows) are shown in the planning images (a–c) acquired with a diagnostic FSPGR that was optimized for Thiel cadaver imaging (FSPGR, TE / TR = 1.8 / 70 ms, FA = 60°, Matrix = 256 × 256, FOV = 30 cm × 30 cm, Slice thickness = 5 mm, NEX = 2). The planning images in (a) and (b) represent sagittal images and (c) an axial oblique image. The iMRI user interface is illustrated in (d) with three different imaging planes frequently updating while a biopsy is performed (PSIF, TE / TR = 3.8 / 7.7 ms, FA = 60°, Matrix = 128 × 128, FOV = 30 cm × 30 cm, Slice thickness = 5 mm). A deep target is successfully punctured with the biopsy gun during near real-time MRI in an axial oblique plane (e) and a shallow target is punctured in an axial plane (f). The orange arrow indicates the needle tip that can be detected from the susceptibility artefact. Note: Targeting was constrained because of trapped air (green arrow) in the abdominal cavity of the cadaver and in particular above the liver. Also, most vessels and organs in a Thiel embalmed cadaver are collapsed due to the absence of perfusion and tissue dehydration



**Fig. 7.** Screenshot acquired on the tablet PC during needle placement with interactive rtMRI guidance (FSPGR, TE / TR = 2.8 / 6.6 ms, FA = 60°, Matrix = 256 × 256, FOV = 30 cm × 30 cm, Slice thickness = 8). An axial oblique plane (left) and a sagittal oblique plane are updated in an interleaved manner for targeting a predefined and existing target area with double oblique needle trajectory

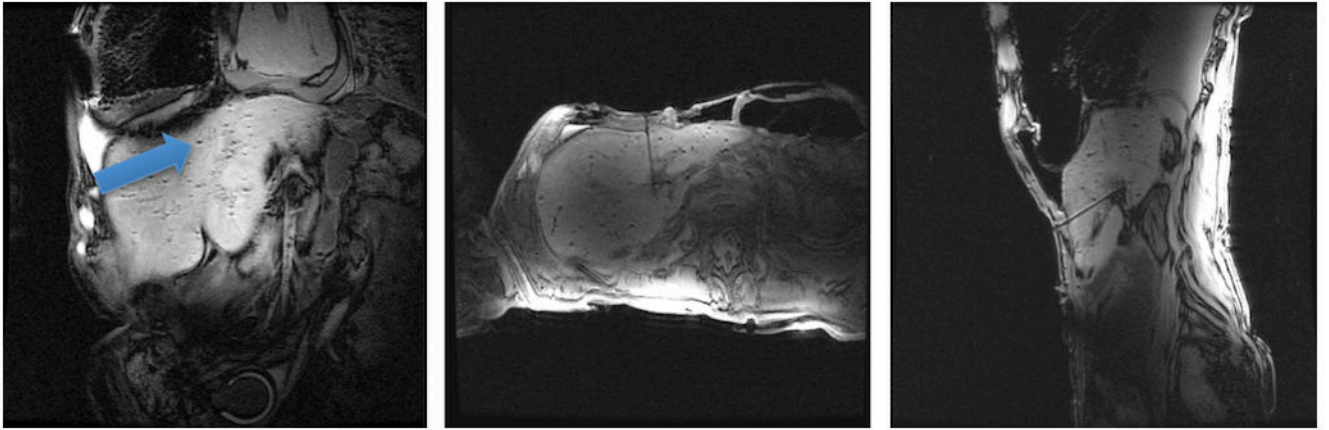


**Fig. 8.**

Verification of correct needle placements in the target (dark) area of the liver a Thiel embalmed cadaver (FSPGR, TE / TR = 3.1 / 70 ms, FA = 60°, Matrix = 384 × 224, FOV = 36 cm × 36 cm, Slice thickness = 4 mm, NEX = 4)

**Table 1**

## Targeting Accuracy and Procedure Time

			<b>3D RMS targeting error (mm)</b>
Phantom – Single Oblique			
	Expert	n =10	1.5 ( $\pm 0.5$ )
	Novice	n =10	2.5 ( $\pm 0.6$ )
Phantom – Double Oblique			
	Expert	n =10	2.5 ( $\pm 0.8$ )
	Novice	n =10	4.0 ( $\pm 1.2$ )
Phantom –All			
	All Paths	n =40	2.8 ( $\pm 1.0$ )
Thiel Cadaver – Double Oblique			
	Expert	n =12	2.9 ( $\pm 0.8$ )
	Novice	n =12	4.1 ( $\pm 0.9$ )

Author Manuscript

Author Manuscript

Author Manuscript

Author Manuscript